JOURNAL OF GENERAL VIROLOGY

RESEARCH ARTICLE

Easton *et al.*, *Journal of General Virology* 2025;106:002190
DOI 10.1099/jgv.0.002190

MICROBIOLOGY SOCIETY

OPEN ACCESS

Identification and characterization of candidate inhibitors of the SARS-CoV-2 nsp14 3′-5′ exoribonuclease

Victoria Easton[1,†], Martin J. McPhillie[2,†], Igor Andrade Santos[1,‡], Philippa Hall[1], C. Patrick McClure[3], Stuart Astbury[4], Emanuelle Paci[1,§], Alexander St John[1,#], Colin W.G. Fishwick[2] and Mark Harris[1,*]

Abstract

Coronaviruses such as SARS-CoV-2 possess the largest positive-sense RNA virus genomes (30 kb). This poses a fidelity problem as the inherent lack of proof-reading capacity of the viral RNA-dependent RNA polymerase results in a high level of mutation. To overcome this issue, coronaviruses encode a 3′–5′ exoribonuclease (ExoN) proof-reading activity, which is a property of a complex of two non-structural proteins nsp14 and nsp10. Inactivating ExoN mutants in SARS-CoV-2 are lethal, indicating the importance of this enzymatic activity for virus replication and raising the possibility that small-molecule inhibitors of ExoN activity could be potential antiviral agents. To evaluate this, we used structure-based drug design approaches to identify potential ExoN inhibitors and tested these for activity against infectious SARS-CoV-2. Two compounds had low micromolar EC_{50} activity and synergized with mutagenic nucleoside analogues. Next-generation sequencing analysis revealed an increased rate of mutation in the presence of these compounds, which is consistent with their mode of action being inhibition of ExoN enzymatic activity.

DATA AVAILABILITY

Sequence reads for all samples have been deposited in the National Center for Biotechnology Information (NCBI) Sequence Read Archive under project ID PRJNA1368746, samples SAMN53368769 - SAMN53368778.

INTRODUCTION

According to the World Health Organisation (WHO) statistics (https://data.who.int/dashboards/covid19/cases), the severe acute respiratory syndrome coronavirus 2 (SARS-CoV-2) pandemic has resulted in the deaths of over 7 million individuals worldwide, with a current cumulative estimate of 778 million infections. Despite an effective vaccination campaign and the declaration from the WHO that the pandemic was over in May 2023, the virus continues to cause a significant number of serious respiratory infections. This is due, at least in part, to the short-term duration of either vaccine-derived or natural immunity, coupled with the continued evolution of the virus. There are few approved therapies for the treatment of patients infected with SARS-CoV-2, highlighting the need for the development of new therapeutic agents that would also be of potential use to combat future spillover events of related viruses.

SARS-CoV-2 has a positive-sense RNA genome of ~30 kb and is classified within the genus *Betacoronavirus* and the species *Betacoronavirus pandemicum* [1]. The size of the coronavirus genome poses a significant issue for the fidelity of genome replication, as the inherent lack of proofreading capacity in the viral RNA-dependent RNA polymerase results in a high level of mutation. This could potentially result in an error catastrophe, whereby the frequency of mutations leads to a loss of function of viral proteins

Received 07 July 2025; Accepted 12 November 2025; Published 19 December 2025
Author affiliations: [1]School of Molecular and Cellular Biology, University of Leeds, Leeds, LS2 9JT, UK; [2]School of Chemistry, University of Leeds, Leeds, LS2 9JT, UK; [3]Wolfson Centre for Global Virus Research, University of Nottingham, Nottingham, NG7 2UH, UK; [4]National Institute for Health Research Nottingham Biomedical Research Centre, University of Nottingham and Nottingham University Hospitals NHS Trust, Nottingham, NG7 2UH, UK.
***Correspondence:** Mark Harris, m.harris@leeds.ac.uk
Keywords: SARS-CoV-2; exoribonuclease; nsp14; small molecule inhibitors.
Abbreviations: ExoN, 3′–5′ exoribonuclease; nsp, non-structural proteins; SGR, subgenomic replicon; WGS, whole-genome sequencing.
‡Present address: The Pirbright Institute, Ash Road, Pirbright, Surrey, GU24 0NF, UK
§Present address: Department of Physics and Astronomy, University of Bologna, Viale Berti-Pichat 6/2, 40125 Bologna BO, Italy
#Present address: Apoha, Nw Works Units 8 & 9, 135 Salusbury Rd, London NW6 6RJ, UK.
†These authors contributed equally to this work
Two supplementary figures and one supplementary table are available with the online version of this article.

and a reduction in infectivity. Coronaviruses overcome this by encoding an exoribonuclease proofreading enzyme [2]. This is a function of one of the 16 non-structural proteins (nsp) encoded by the genome: nsp14. In complex with nsp10 (Fig. 1a), nsp14 possesses two enzymatic activities – a 3′–5′ exoribonuclease (abbreviated to ExoN hereafter) and a methyltransferase that plays a role in capping of viral mRNAs. The ExoN activity can excise misincorporated bases from the 3′ end of the nascent RNA strand during genome replication, allowing the polymerase (a complex of nsp12, nsp7 and nsp8) to replace this with the correct base [3]. As well as reducing the error rate of coronavirus RNA synthesis, the ExoN also results in resistance to mutagenic nucleoside analogues such as ribavirin. In this regard, the ExoN has been proposed as a potential target for the development of antiviral agents [4]. Effective ExoN inhibitors would increase the mutation rate, leading to error catastrophe. Genetic analysis supports the requirement for active nsp14 ExoN activity during the coronavirus lifecycle, as inactivating point mutations in nsp14 result in a lethal loss of infectivity for MERS and SARS-CoV-2 [5], although they only reduced infectivity by fourfold for SARS-CoV [6] or murine hepatitis virus [7].

Given the critical requirement for ExoN activity, we used an *in silico* virtual screening platform to identify small molecules with the potential ability to bind to the ExoN active site of SARS-CoV-2 nsp14. These compounds were then tested for the ability to block the production of infectious SARS-CoV-2. One of these, designated CB3, and a derivative (CB3-1), exhibited low micromolar EC_{50} activity and were further shown to synergise with mutagenic nucleoside analogues. Next-generation sequencing analysis

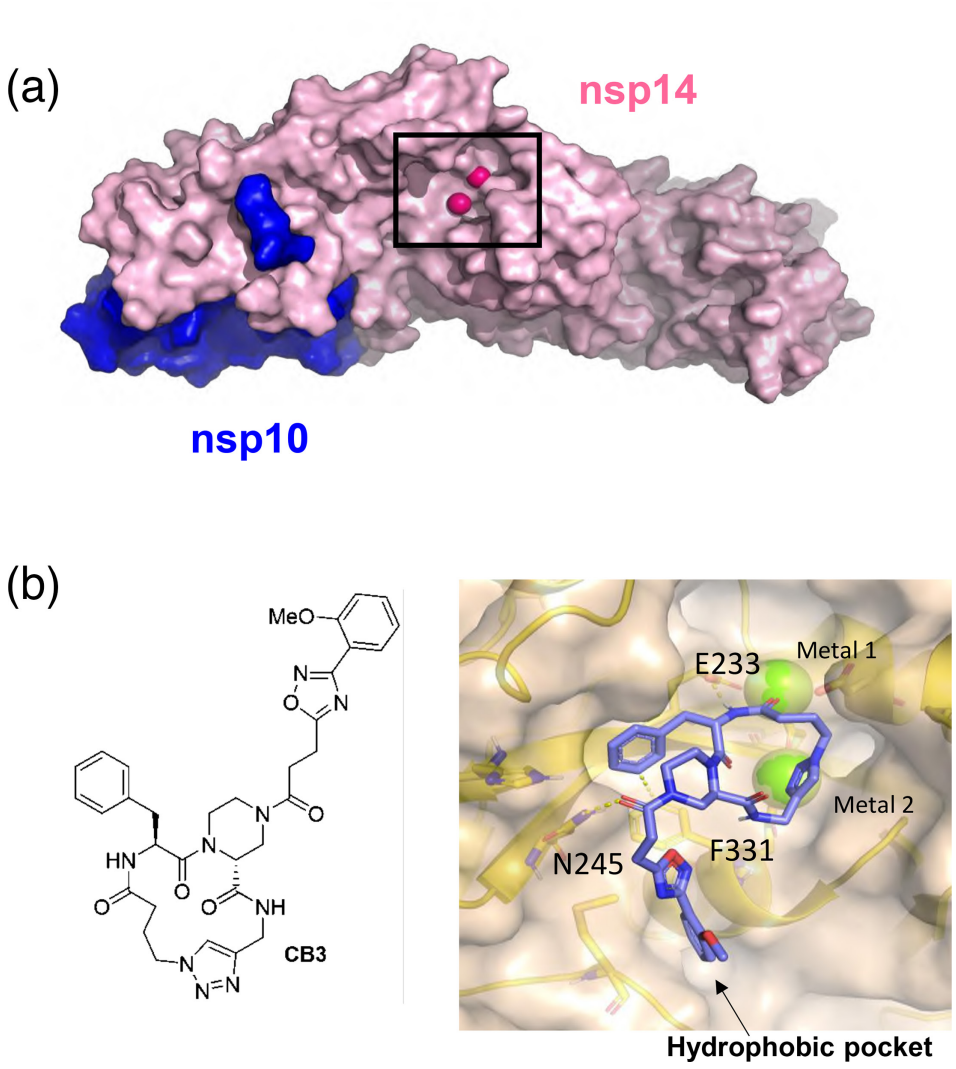

Fig. 1. Structure of the SARS-CoV nsp14:nsp10 complex. (a) Surface representation of the SARS-CoV nsp14 (pink) nsp10 (blue) complex, illustrating the exoribonuclease active site with two coordinated metal ions (hot pink). Image generated using PyMol from PDB:5C8U. (b) Chemical structure of lead compound CB3 with a representation of the docking of CB3 into the nsp14 ExoN active site.

revealed an increased rate of mutation in the presence of CB3 or CB3-1, which is consistent with the mode of action being inhibition of ExoN enzymatic activity.

METHODS

Cell lines

A549-AT human lung adenocarcinoma alveolar basal epithelial cells, which express the ACE2 and TMPRSS2 receptors (sourced from the Centre for AIDS Research, National Institute for Biological Standards and Control (NIBSC) (part of the Medicines and Healthcare products Regulatory Agency), UK, catalogue number 101004), and baby hamster kidney (BHK-21) cells, were maintained in Dulbecco's Modified Eagle's Medium (Sigma-Aldrich, UK), supplemented with penicillin (100 U ml^{-1}), streptomycin (100 mg ml^{-1}), non-essential amino acids (1% v/v) (all from Gibco Life Technologies, Thermo-Fisher, UK) and FBS (10% v/v; Hyclone, Logan, UT, USA), under standard incubation conditions at 37 °C in a humidified 5% CO_2 atmosphere. Additionally, A549-AT cells were grown with the addition of Geneticin (G418, Invitrogen, UK) at 2 mg ml^{-1} and Hygromycin B (Sigma-Aldrich, UK) at 200 µg ml^{-1}, as described [8].

Compounds

Compounds were purchased from ChemBridge via their Hit2Lead platform (https://www.hit2lead.com/search.asp). Compounds were tested for purity via LC-MS to confirm their molecular mass as a single peak. Compounds with <90% purity via this check were discarded. Using the SAR-by-inventory approach, 48 similar compounds to CB3 were available for purchase from ChemBridge. Keeping the macrocycle core consistent, four compounds (ChemBridge IDs 98191080, 76506023, 27512028, 37731775 – renamed CB3-1 to CB3-4) were selected to probe a small hydrophobic pocket in the proposed binding site. These were checked for purity as described above.

Virtual screening cascade

Virtual screening was performed using Schrodinger's Glide software and the Maestro GUI and a homology model of ExoN was generated in-house. Various libraries (i.e. Drugbank and our proprietary in-house collection) were screened, including the ChemBridge coronavirus library of ~16,000 structures [9], from which our hit compounds were identified. Libraries were screened on vHTS then SP modes, with the top 10% of compounds from each screening run taken to the next step (with default settings). Compounds were selected for biological evaluation based on three factors: Glide docking score, visual inspection of the ligand conformation and predicted intermolecular interactions with the protein. Docking files for the top-ranked compounds using the ChemBridge library are available on request.

SARS-CoV-2 viruses

The parental Wuhan-like SARS-CoV-2 isolate England/02/2020 (GISAID access number EPI_ISL_407073) was isolated and characterized at the Francis Crick Institute (UK) and kindly provided by Public Health England. Virus was propagated in Vero E6-ACE2 cells, titres were determined using the $TCID_{50}$ method and calculated by the Spearman and Kärber algorithm as described [10]. All procedures with infectious SARS-CoV-2 were performed under BSL3 conditions.

Single-cycle replication assay

A549-AT cells (1×10^4) were seeded into 96-well plates in culture medium and incubated overnight. The medium was aspirated and replaced with medium containing a range of concentrations (1 nM–100 µM) of either CB3/CB3-1, the mutagenic nucleoside analogues ribavirin or molnupiravir or the chain terminator remdesivir. A stock of SARS-CoV-2 (England/02/2020) was then titrated by $TCID_{50}$ assay at each concentration of the compounds, with four replicates at each virus dilution. Virus replication was allowed to proceed for 4 days before cytotoxicity was determined visually. A DMSO control was included in each $TCID_{50}$ 96-well plate, and the data are presented as a percentage of this titre.

Multiple-cycle replication assay

A549-AT cells (2×10^5) were seeded into 6-well plates in culture medium and incubated overnight. The medium was aspirated and replaced with specific dilutions of test compounds diluted in culture media, prior to relocation to the BSL3 laboratory. SARS-CoV-2 (England/02/2020) (multiplicity of infection (MOI) 0.01) was added to each well and incubated for 4 days (37 °C, 5% CO_2); each 6-well plate contained a DMSO control. Cells and supernatant were harvested and either processed for $TCID_{50}$ assay as described or stored at −80 °C if not used immediately.

SARS-CoV-2 subgenomic replicon assay

The SARS-CoV-2 subgenomic replicon (SGR) plasmid pCCL-4K-SARS-CoV-2-Repl-PL-mNeonGreen was used in this study. This SGR has a deletion of the region encoding for spike, membrane and accessory proteins 3a, 3b, E, 6, 7a and 7b (positions 21565 to 28124 of the SARS-CoV-2 Wuhan strain genome) (kind gift from Prof. Andres Merits, University of Tartu, Estonia). The transcription of replicon-competent RNA containing the mNeonGreen reporter gene is driven by the CMV promoter, and the expression of the reporter is proportional to subsequent viral RNA replication and translation. For the assay, BHK-21 cells were seeded in 48-well plates at 5×10^4 cells well^{-1}. After 24 h, cells were transfected with 600 ng of the plasmid per well and 4 h post-transfection were treated with Remdesivir in the presence or absence of the single-cycle EC_{50} concentrations (2.2 µM and 1.8 µM respectively). DMSO 0.1% was used as a vehicle control. After 72 h incubation, the plates were placed in an IncuCyte® S3 Live-Cell Analysis System (Sartorius AG, DE), and green fluorescence was observed at 10× objective. The images were recorded and analysed employing the basic analyser from the IncuCyte S3 system to obtain the total green integrated intensity of the fluorescence (GCU × µm^2 well^{-1}). Impact on viral replication was calculated according to the equation $(T/C) \times 100\%$, in which T and C represent the optical density of the compound-treated and control (DMSO-treated) wells.

Preparation of samples for SARS-CoV-2 sequencing

Cells were infected with SARS-CoV-2 (England/02/2020) at an MOI of 0.1 either in the presence of an EC_{90} of molnupiravir alone, or with CB3 or CB3-1 at the single-cycle EC_{50} concentrations (2.2 µM and 1.8 µM, respectively). After 24 h, supernatant from infected cells was collected, and total RNA in the supernatant was extracted using the QIAGEN viral RNA mini extraction kit following the manufacturer's instructions. The resulting RNA of each sample was submitted to sequencing as described [11]. Briefly, cDNA was prepared with RNA to cDNA EcoDry™ Premix with random hexamers (Takara Bio) following the manufacturer's instructions and then processed similarly to previously described [12]. Briefly, cDNA was used as template in a PCR reaction assembled with Q5® High-Fidelity 2X Master Mix (New England Biolabs, UK) and either primer set 1 (odd-numbered primer pairs) or 2 (even-numbered primer pairs) of either targeting individual coronaviral species or all five combined at a final concentration of 0.015 µM. PCR reactions were as follows: 98 °C for 30 s, then 32 cycles of 98 °C for 15 s and 65 °C for 5 min. The PCR products were inspected for specificity and yield on a 2% agarose gel with ethidium bromide, combined and quantified using Qubit. Amplicons were prepared and barcoded using the SQK-LSK109 and EXP-NBD196 kits, respectively (Oxford Nanopore), and sequenced on an Oxford Nanopore GridION as previously described [11].

Variant calling

For an indication of mutation rates vs. the reference sequence, nanopore reads were aligned to the Wuhan-Hu-1 SARS-CoV-2 reference genome (NC_045512.2), using Minimap2 [13]. Primer sequences were trimmed from alignments using the ARTIC align_trim script (https://github.com/artic-network/fieldbioinformatics) and primer-trimmed alignments were used as the input for iVar [14], with the minimum quality score threshold set at 5 and a minimum depth of 20 required to call a variant.

RESULTS

To facilitate the rapid testing of compounds, we used our in-house library of compounds (~27 K), the DrugBank library of clinical and pre-clinical candidates (~8.7 K) and the ChemBridge coronavirus screening library (~16 K) in our virtual screening campaign. No suitable compounds were identified during the virtual screens of the in-house and DrugBank libraries. The ChemBridge coronavirus library had been compiled from their main 1.3M collection using the Virtual Flow methodology [9]. This library contained putative inhibitors for 17 coronavirus and host cell targets, which were subsequently filtered down to only include compounds identified as a putative nsp14 hit (~1.750 compounds). These compounds were then subjected to the ligand preparation process in Maestro (changing the default pH setting to 7.0±0.5) to generate multiple conformers as required (~5.2 K). At the start of this work, there were no available protein databank (PDB) structures of the SARS-CoV-2 nsp14 in complex with nsp10, and so a homology model was built using Modeller 9.23 [15]. The model was based on the SARS-CoV nsp14:10 structure, which shares 95% homology with SARS-CoV-2 nsp14:10. One of the Mg^{2+} ions was missing from the crystal structure and was added manually by positioning within the region of high density observed from co-solvent free-energy maps obtained from MD simulations with Mg^{2+} ions. The homology model used and the structure of the SARS-CoV-2 nsp10 complexed with the nsp14 ExoN domain [16] (7DIY) are virtually identical (C-alpha RMSD below 0.6 Å and four Zn ions in the same positions), whilst the Mg^{2+} is absent in 7DIY. Additional MD simulations were performed using Amber [17] to generate diverse structural ensembles for docking using both the nsp14:nsp10 starting structure and nsp14 alone. Two putative binding sites were explored: the nsp14 active site around the metal ions and the nsp14:nsp10 protein–protein interface. Forty-one compounds were purchased and tested at a single concentration (10 µM) for the ability to inhibit replication of the Wuhan-like SARS-CoV-2 isolate England/02/2020 (EPI_ISL_407073) in a single-cycle $TCID_{50}$ assay on A549-AT cells (expressing ACE2 and TMPRSS2). In this assay, inhibition of SARS-CoV-2 replication was determined by a reduction in measured $TCID_{50}$ titre in the presence of a compound, compared

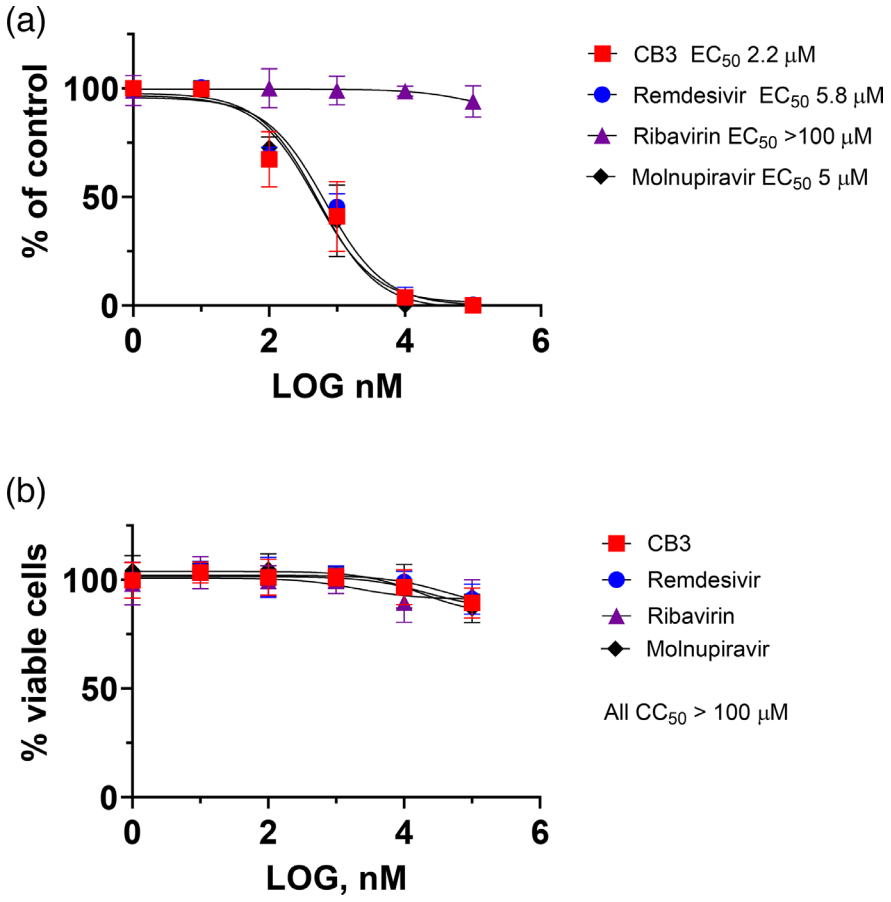

Fig. 2. Activity of CB3 assayed in a single replication cycle. (a) Dose response curve. SARS-CoV-2 isolate England/02/2020 (EPI_ISL_407073) was titrated by $TCID_{50}$ assay on A549-AT cells in the presence of a range of concentrations (1 nM–100 μM) of CB3. $TCID_{50}$ titres were read manually at 120 hours post infection (h.p.i.). The resulting titres were normalized to the titre in the absence of CB3 and presented as a percentage of that value (*n*=3). Average titres were plotted from three independent experiments performed in triplicate and EC_{50} values were calculated by GraphPad Prism software. (b) Cytotoxicity was determined by MTT assay, following incubation of A549-AT cells in the presence of the indicated concentration of CB3 for 24 h. Error bars show SD.

to the vehicle (DMSO) control. Seven compounds displayed >50% inhibition (Table S1, available in the online Supplementary Material); of these, CB3 displayed the most promise and was predicted to bind to the nsp14 active site (Fig. 1b).

To determine the potency of CB3, a stock of SARS-CoV-2 (England/02/2020) was titrated by $TCID_{50}$ assay on A549-AT cells in the presence of a range of concentrations (1 nM–100 μM) of CB3. As controls, the titrations were performed in the presence of the same concentrations of the mutagenic nucleoside analogues ribavirin and molnupiravir or the chain terminator remdesivir. As shown in Fig. 2a, CB3 effectively inhibited replication of SARS-CoV-2 with an EC_{50} of 2.2 μM and EC_{90} of 8.1 μM (Table 1), similar to both remdesivir and molnupiravir. As expected, ribavirin was not able to inhibit SARS-CoV-2 replication. None of the compounds tested exhibited any cytotoxicity after 24 h incubation at 100 μM (Fig. 2b). In addition, we evaluated the cytotoxicity of CB3 over a 96-h incubation (Fig. S1); reassuringly, it also did not show any cytotoxicity in this assay.

Encouraged by these initial findings, we sought to establish the preliminary structure-activity relationship (SAR) of CB3 using an SAR-by-inventory approach. Keeping the macrocyclic core consistent, we focused on the 'side-arm', varying the terminal aromatic group that was predicted to bind into the hydrophobic pocket of nsp14 (Fig. 1b), seeking to improve binding. Four derivatives (CB3-1 to CB3-4, Fig. 3a) were obtained from commercial sources and tested for activity at a single concentration (CB3 EC_{50}, 2.2 μM). As shown in Fig. 3b, only CB3-1 retained any anti-SARS-CoV-2 activity, which was unexpected given the similarity in both the alkyl linker length and the size of the terminal aromatic group between CB3-1 and CB3-3. This suggested that the interaction of these compounds with the hydrophobic pocket may be critical for ExoN inhibition. We proceeded to determine the EC_{50} value of CB3-1 (Fig. 4a); this was slightly lower than CB3 (1.8 μM). This was reflected in the corresponding EC_{90} values (Table 1). CB3-1 did not exhibit any cytotoxicity at concentrations up to 100 μM when assayed at either 24 h (Fig. 4b) or 96 h (Fig. S1).

Table 1. Summary of EC_{50} and EC_{90} data

Assay	Compound	EC_{50} (μM)	EC_{90} (μM)
Single cycle	CB3	2.2	8.1
(Figs 2 and 4)	CB3-1	1.8	7.9
	Remdesivir	5.8	9.8
	Molnupiravir	5.0	9.7
	Ribavirin	>100	>100
Multiple cycle	CB3	0.8	58
(Fig. 5)	CB3-1	0.5	N/A
	Remdesivir	1.3	10.2
	Molnupiravir	1.0	12.0
	Ribavirin	>100	>100

N/A: could not be calculated as plateaued above 90% inhibition values.

We reasoned that the titration assay used in Figs 2 and 4, whilst convenient and rapid, did not allow us to determine the efficacy of CB3 and CB3-1 in the context of the entire lifecycle of the virus, including virus production. We, therefore, utilized a multiple replication cycle assay in which cells were infected with SARS-CoV-2 at an MOI of 0.01 and treated with compounds for 24 h. Cell culture supernatants were then harvested and titrated by $TCID_{50}$ assay, allowing us to measure production of infectious virus and any effect thereupon by the compounds. As shown in Fig. 5, this assay demonstrated a modest improvement in the EC_{50} values for all compounds, with both CB3 and CB3-1 performing as well as remdesivir and molnupiravir. Ribavirin remained inactive in this assay. However, it is noteworthy that the EC_{90} value for CB3 was significantly higher than in the single-cycle assay (Table 1), and in the case of CB3-1, it could not be calculated as the inhibitory curve plateaued before 90%.

As well as removing misincorporated natural nucleosides, the ExoN is able to contribute to resistance to mutagenic nucleoside analogues [18] as well as chain-terminating nucleosides [19]. We, therefore, proceeded to evaluate whether CB3 and/or CB3-1 were able to increase the sensitivity of SARS-CoV-2 replication to mutagenic nucleoside analogues. To test this, A549-AT cells were infected with SARS-CoV-2 at an MOI of 0.01 prior to combination treatment with CB3 or CB3-1 at the previously defined EC_{50} (0.8 or 0.5 μM, respectively; see Fig. 5), together with a titration of ribavirin, molnupiravir or remdesivir at values between 1 nM and 100 μM. We also included remdesivir as this nucleoside analogue has been shown to function as a chain terminator, rather than a mutagen. Supernatants from these cells were harvested and titrated by $TCID_{50}$ assay as described above. The addition of CB3 (Fig. 6a) or CB3-1 (Fig. 6b) at their respective EC_{50} values dramatically increased the potency of the three nucleoside analogues. The increased potency differed between the three analogues: for molnupiravir, we observed an approximate 20-fold increase (1 μM alone to 49/62 nM in the presence of CB3/CB3-1), whereas remdesivir exhibited a 260-fold increase (1.3 μM alone to 5 nM in the presence of CB3/CB3-1) (compare with the EC_{50} values for the nucleoside analogues alone shown in Fig. 5). This was surprising as remdesivir has been reported to induce delayed chain termination after incorporation of an additional three bases, suggesting that it would be resistant to ExoN excision [20], although other *in vitro* studies have shown that remdesivir can be excised by nsp14 [12]. Remarkably, ribavirin also exhibited antiviral activity in the presence of CB3 or CB3-1. Ribavirin alone had no antiviral activity even at the highest concentration tested (100 μM), whereas in the presence of CB3 or CB3-1, it exhibited an EC_{50} value of 0.5 or 0.3 μM. No cytotoxicity was observed for any of the compound combinations (CC_{50} values all >100 μM) (Fig. 6c).

To verify that CB3 and CB3-1 were acting at the stage of genome replication, we evaluated their activity using a SARS-CoV-2 sub-genomic replicon system. A DNA construct containing the entire genome of the Wuhan strain of SARS-CoV-2 in which the fragment encoding Spike through to ORF7b was replaced with the mNeonGreen reporter was obtained from Prof. Andres Merits (University of Tartu) [21]. Following transfection of this plasmid into BHK-21 cells, replication was evaluated in real time by measuring mNeonGreen expression using an Incucyte S3 live cell imaging system (Fig. 7, representative images shown in Fig. S2). CB3 or CB3-1 was added at the previously defined EC_{50} from the single-cycle experiment (2.2 or 1.8 μM, respectively; see Figs 2 and 4). Remdesivir exhibited an EC_{50} value of 2.3 μM in the replicon system, similar to that obtained in the context of infectious virus (1.3 μM) (Fig. 5). Although it should be noted that the shape of the curves for remdesivir+CB3 or CB3-1 only allows an estimate of the EC_{50} values as they do not plateau, regardless of this both compounds significantly enhanced the EC_{50} value of remdesivir (to 0.18 and 0.12 μM, respectively, an increase in sensitivity of 12.8- or 19.2-fold) (Fig. 7).

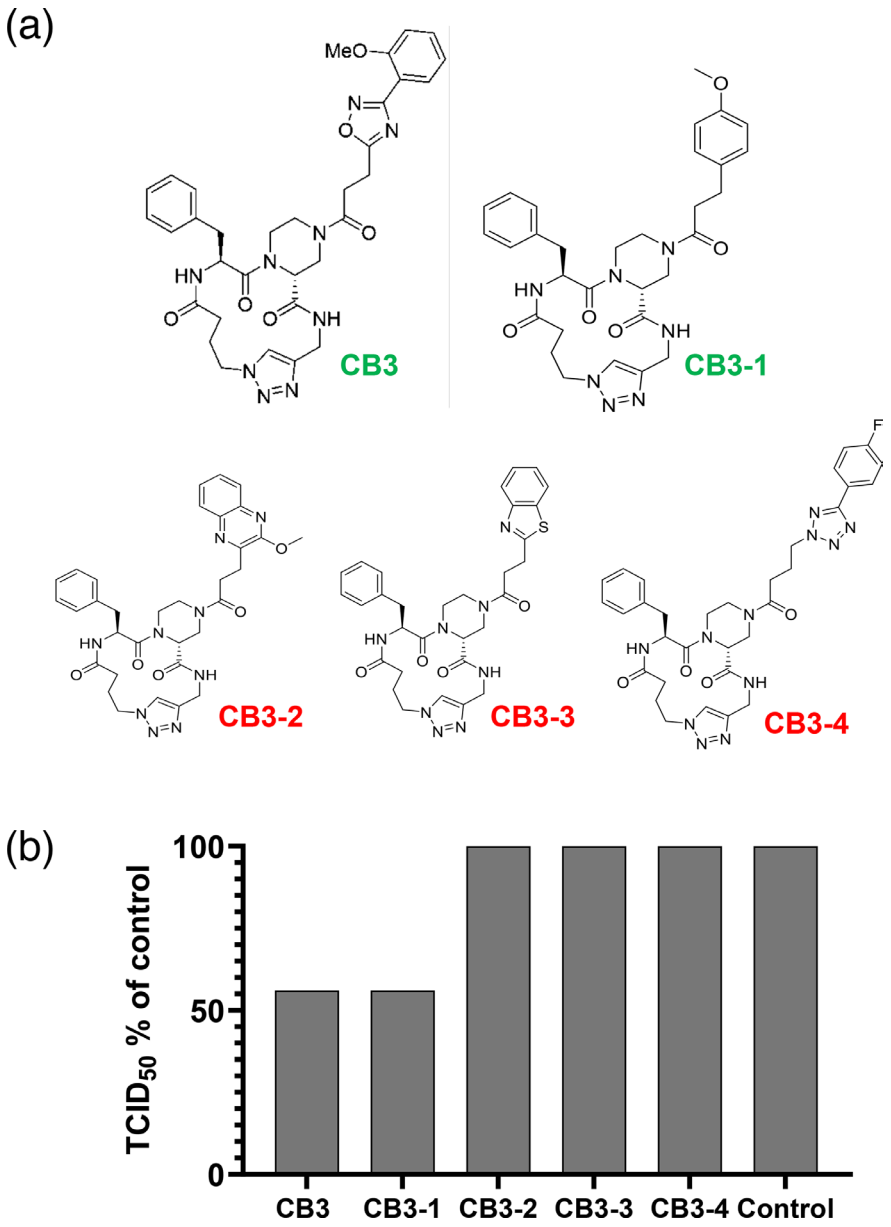

Fig. 3. SAR analysis of CB3. (a) Chemical structure of lead compound CB3 and four derivatives (CB3-1, CB3-2, CB3-3 and CB3-4) investigated for SAR analysis. CB3 and CB3-1 are indicated in green as active compounds; the others are in red as inactive. (b) Initial screening of derivative activity in a single replication cycle. SARS-CoV-2 isolate England/02/2020 (EPI_ISL_407073) was titrated by $TCID_{50}$ assay on A549-AT cells in the presence of CB3 and derivatives at the EC_{50} of CB3 (2.2 µM). $TCID_{50}$ titres were read manually at 120 h.p.i. The resulting titres were normalised to the titre in the absence of CB3 and presented as a percentage of that value (*n*=1).

Lastly, we sought to provide evidence for the mode of action of CB3 and CB3-1 by determining the frequency of mutations in the genome of SARS-CoV-2 following treatment with the mutagenic nucleoside analogue molnupiravir with or without the putative ExoN inhibitors. Molnupiravir is a prodrug and the active derivative β-D-N^4-hydroxycytidine (NHC) has been shown to compete with CTP or ATP for incorporation into a growing RNA strand, resulting in an increased rate of G->A and C->U transitions [22]. We predicted that by preventing the removal of NHC from nascent SARS-CoV-2 genomes, CB3 or CB3-1 would increase the rate of G->A and C->U transitions in the resulting virus population. A proviso was that if the rate of transitions was increased dramatically, it would result in an error catastrophe and might not be represented in the pool of infectious viruses released from the cells. To test this, we infected A549-AT cells with SARS-CoV-2 at an MOI of 0.1, treated with an EC_{90} of molnupiravir with or without CB3 or CB3-1 at the single-cycle assay EC_{50} concentrations and harvested cell supernatants at 24 h.p.i. RNA was extracted and subjected to cDNA synthesis and whole-genome sequencing

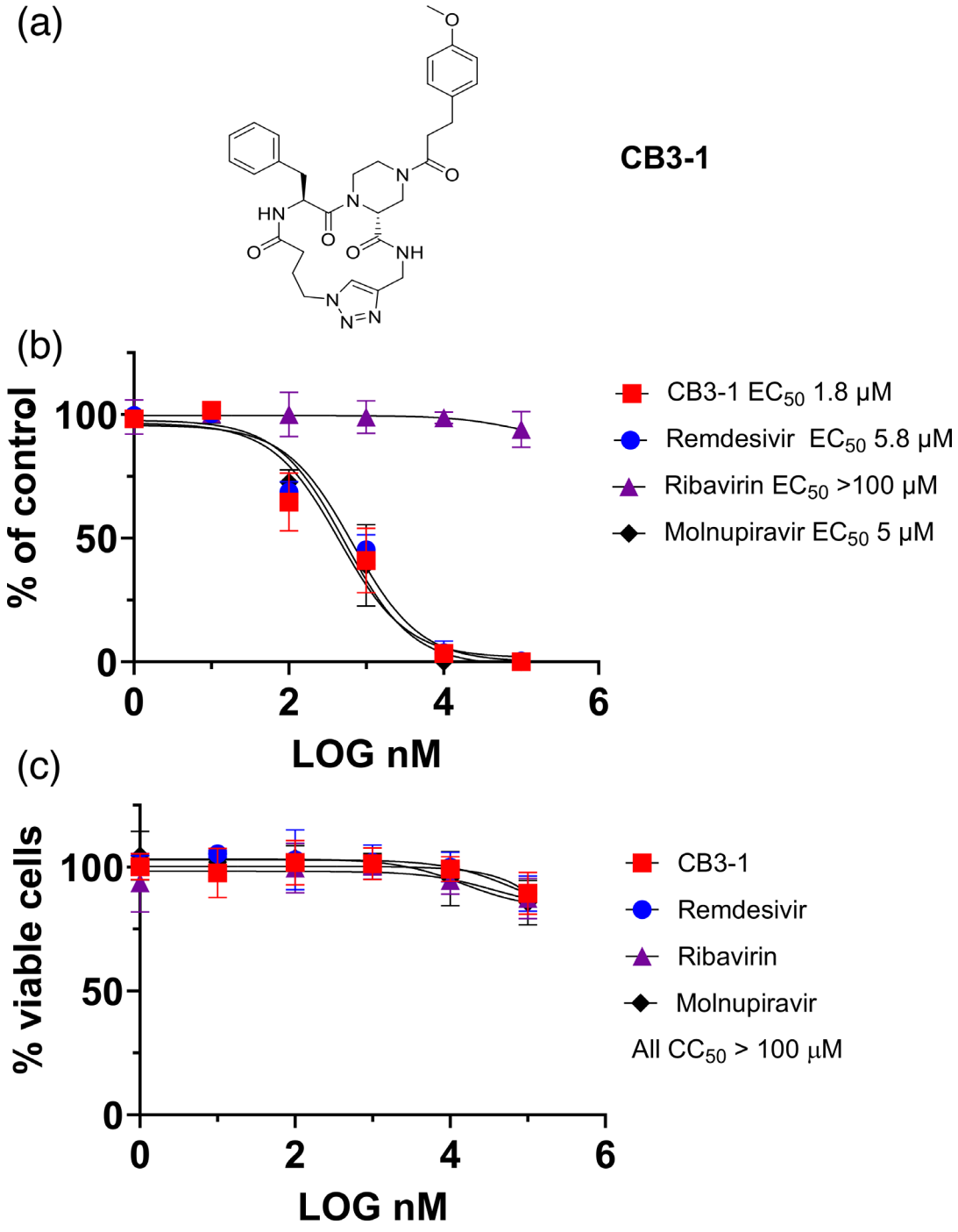

Fig. 4. Activity of CB3-1 assayed in a single replication cycle. (a) Structure of CB3-1. (b) SARS-CoV-2 isolate England/02/2020 (EPI_ISL_407073) was titrated by $TCID_{50}$ assay on A549-AT cells in the presence of a range of concentrations (1 nM–100 µM) of CB3-1. $TCID_{50}$ titres were read manually at 120 h.p.i. The resulting titres were normalized to the titre in the absence of CB3 and presented as a percentage of that value (n=3). Average titres were plotted from three independent experiments performed in triplicate, and EC_{50} values were calculated by GraphPad Prism software. (c) Cytotoxicity was determined by MTT assay, following incubation of A549-AT cells in the presence of the indicated concentration of CB3-1 for 24 h. Error bars show SD.

(WGS) using a bespoke set of primers [23]. The resulting dataset was analysed to determine the number and frequency of G->A and C->U transitions compared to the input sequence (Fig. 8). Although the numbers are low, there is a clear trend towards increased mutagenesis in the presence of CB3 or CB3-1 (Fig. 8a); in particular, CB3-1 exhibited a twofold increase in the mutation rate. Treatment with molnupiravir alone resulted in two detected U->C transitions, one C->U but no G->A, whereas the presence of CB3 or CB3-1 increased the number of C->U transitions to three/four, respectively, and resulted

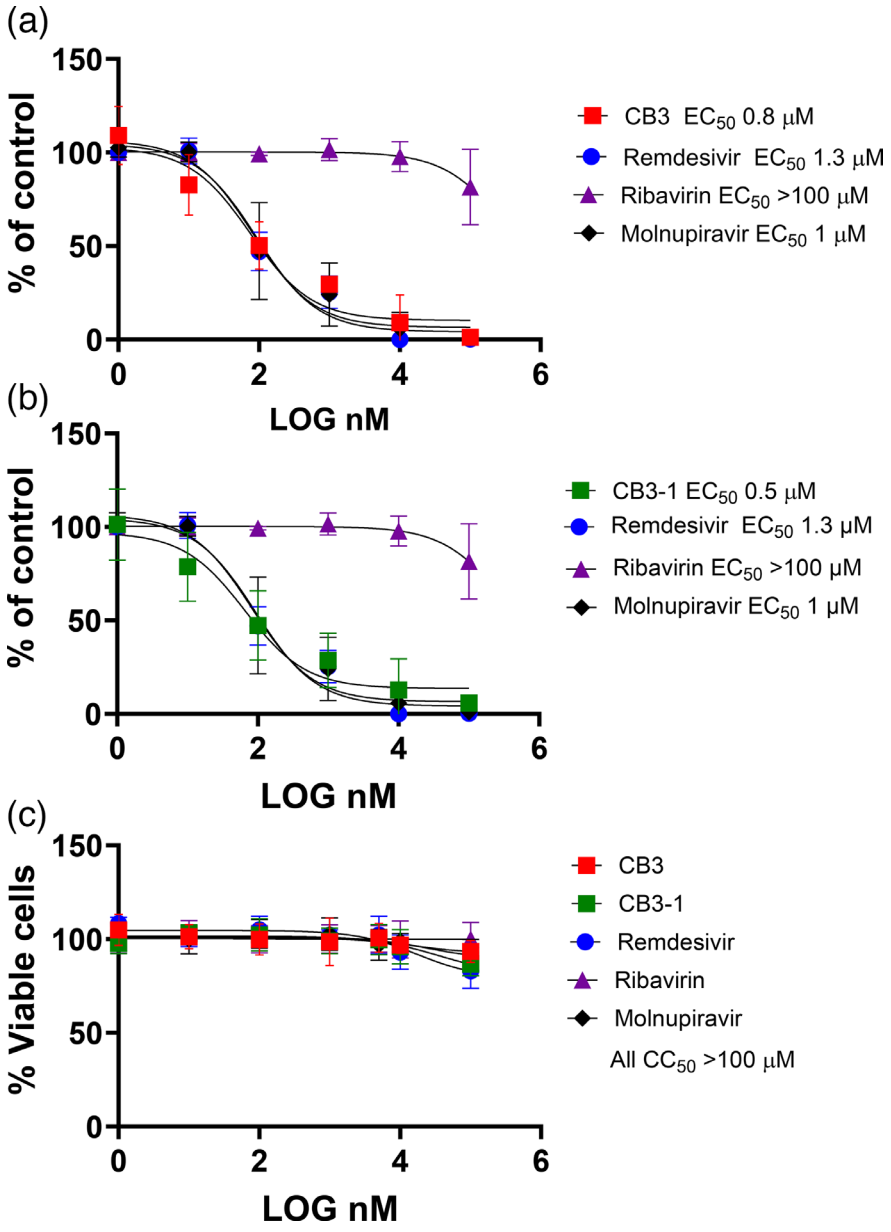

Fig. 5. Activity of CB3 and CB3-1 in a multiple-cycle assay. (a, b) A549-AT cells were infected with SARS-CoV-2 at an MOI of 0.01 prior to treatment with CB3 (a), CB3-1 (b), ribavirin, remdesivir or molnupiravir at the indicated concentrations for 24 h. Cell culture supernatants were then harvested and titrated by $TCID_{50}$ assay. The resulting titres were normalized to the titre in the absence of compound and presented as a percentage of that value (*n*=3). (c) Cytotoxicity was determined by MTT assay, following incubation of A549-AT cells in the presence of the indicated concentration of CB3, CB3-1, ribavirin, remdesivir or molnupiravir for 24 h. Error bars show SD.

in one or three G->A transitions (Fig. 8b). When presented as a mutation rate per 10,000 nt (Fig. 8c/d), the CB3/CB3-1 mediated increases in C->U transitions are statistically significant, whereas the increases in G->A fall below the level of significance. Taken together, these data are consistent with the hypothesis that the mode of action of CB3 and CB3-1 is to inhibit the exoribonuclease activity of nsp14.

DISCUSSION

In this paper, we describe the use of *in silico* drug design methodology to identify potential small-molecule inhibitors of SARS-CoV-2 nsp14 ExoN. Although there is a large literature describing potential small-molecule inhibitors of nsp14, the majority of these target the methyltransferase activity. A number of papers have described ExoN inhibitors; although most of these have

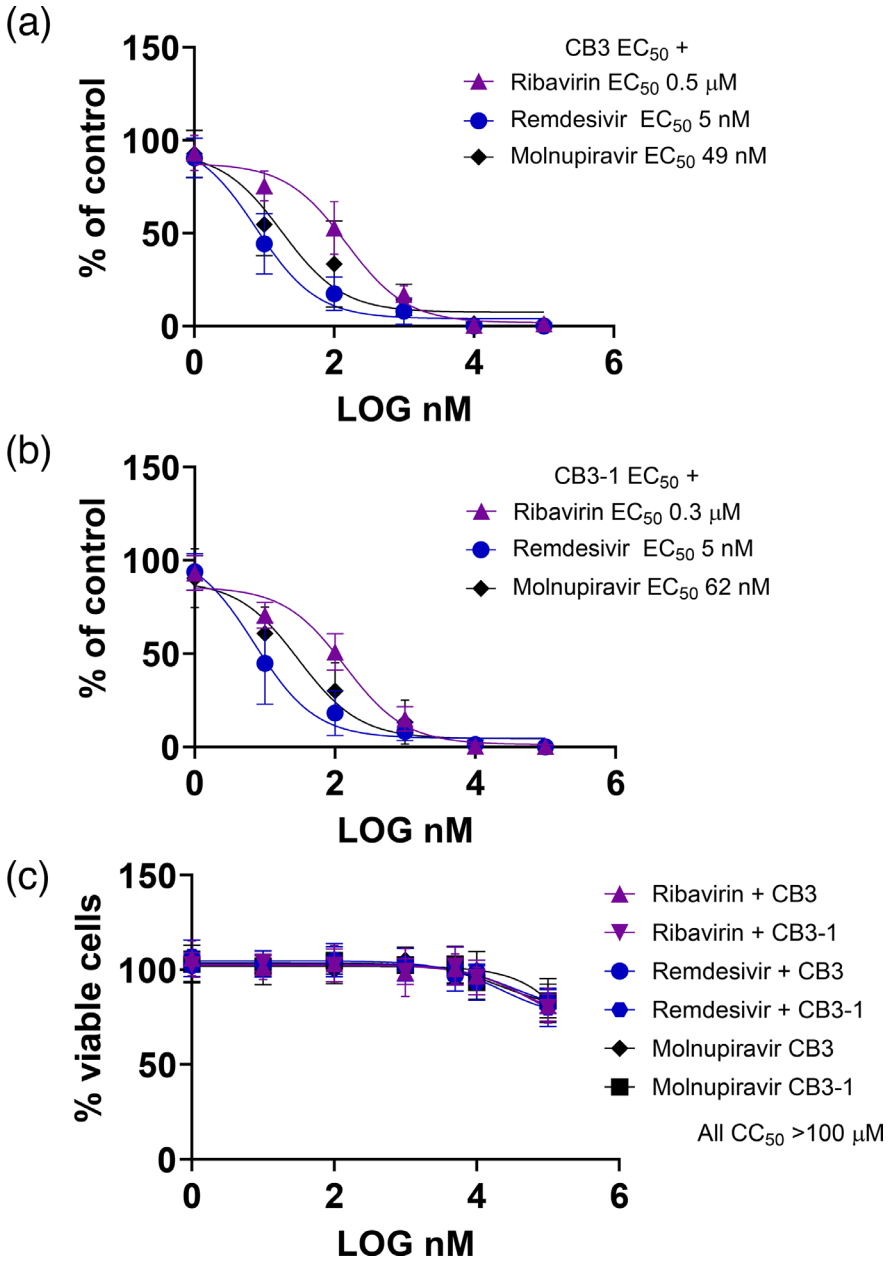

Fig. 6. Combination of CB3/CB3-1 with mutagenic nucleoside analogues. (a, b) A549-AT cells were infected with SARS-CoV-2 at an MOI of 0.01 prior to treatment with CB3 (a) or CB3-1 (b) alone at the previously defined EC_{50} from the multiple-cycle assay (0.8 or 0.5 µM, respectively, see Fig. 5) or in combination with the indicated concentrations of ribavirin, remdesivir or molnupiravir for 24 h. Cell culture supernatants were then harvested and titrated by $TCID_{50}$ assay. The resulting titres were normalized to the titre obtained with CB3 or CB3-1 alone in the absence of the mutagenic nucleosides and presented as a percentage of that value (n=3). Average titres were plotted from three independent experiments performed in triplicate and EC_{50} values were calculated by GraphPad Prism software. (c) Cytotoxicity was determined by MTT assay, following incubation of A549-AT cells in the presence of CB3 or CB3-1 together with the indicated concentration of ribavirin, remdesivir or molnupiravir for 24 h. Error bars show SD.

focused on screening of repurposed drugs [24–26], some novel compounds have also been identified [27, 28]. Intriguingly, it has also been demonstrated that inhibitors of the hepatitis C virus NS5A protein, such as pibrentasvir or ombitasvir, can also act as nsp14 ExoN inhibitors both *in vitro* and *in vivo* [29], although these compounds exhibited low micromolar EC_{50} (0.7 µM) when assayed against SARS-CoV-2, as compared to low picomolar EC_{50} in the context of HCV infection.

It is interesting to speculate whether nsp14 mutations might result in resistance to CB3/3-1. As the compounds were designed to bind to the active site, and nsp14 ExoN function is critical for SARS-CoV-2 replication [5], it seems unlikely that active site mutants would retain replicative fitness and thus become resistant. Of note, a recent study [30] identified a number of naturally

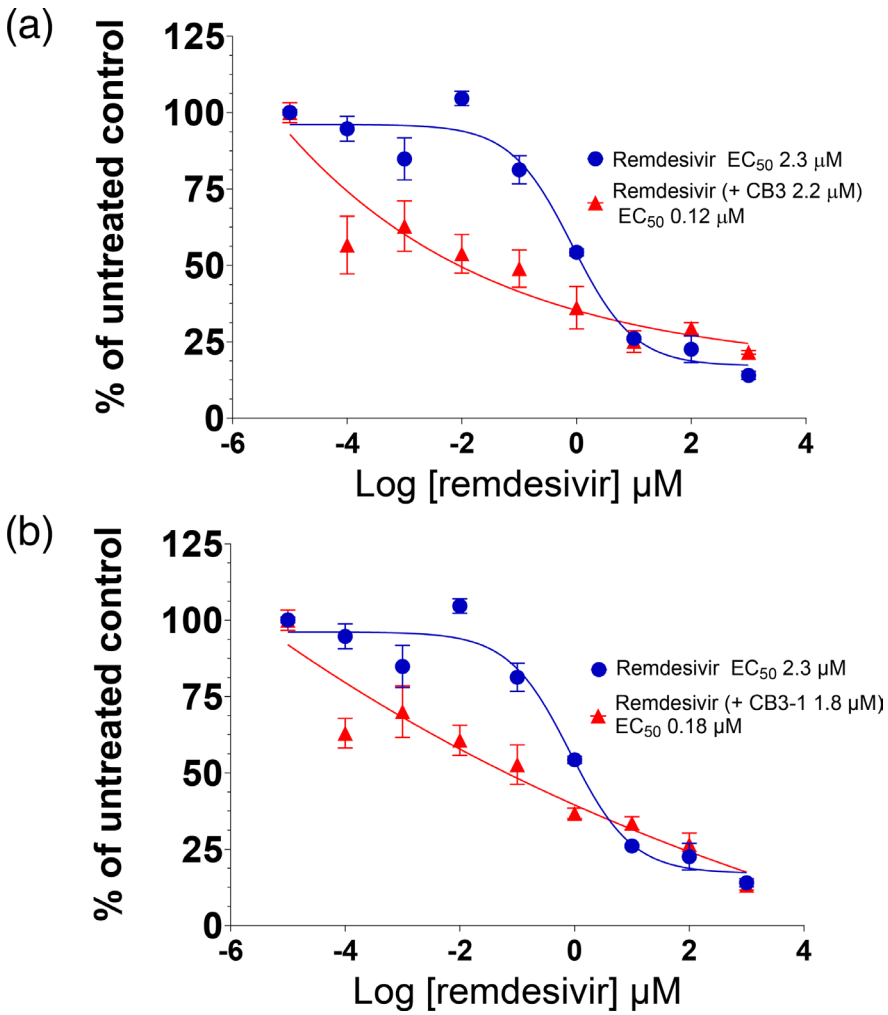

Fig. 7. Activity of CB3/CB3-1 in a SARS-CoV-2 sub-genomic replicon system. BHK-21 cells were transfected with a DNA plasmid containing the entire SARS-CoV-2 cDNA in which the Spike to ORF7b coding sequence was replaced by mNeonGreen. Cells were treated with the indicated concentrations of remdesivir either alone or in the presence of CB3 at 2.2 μM (a) or CB3-1 at 1.8 μM (b). Replication was assayed by measuring the number of mNeonGreen-positive cells on an Incucyte S3 live cell imaging system at 72 hours post transfection (h.p.t.). The resulting values were normalized to the value in the absence of remdesivir and presented as a percentage of that value (n=3). Error bars show SD.

occurring nsp14 amino acid substitutions that were associated with higher genomic mutation rates, in particular P203L. However, this residue is at the interface between nsp14 and nsp10, and the other amino acids (including L177, S369 and M501) were also distal to the CB3/3-1 binding site. Thus, it also seems unlikely that mutations at these sites would result in resistance to CB3/3-1; indeed, by perturbing nsp14 ExoN activity, they might synergise with CB3/3-1. On a related point, the addition of CB3-1 increased the molnupiravir-induced mutation rate 2-fold (Fig. 8a), similar to the increase observed for the P203L virus [30]. Whilst this seems modest, it is likely that higher mutation rates would be lethal.

One possible outcome of the use of nsp14 ExoN inhibitors would be an increase in the particle-to-infectivity ratio of virus, due to the presence of increased numbers of lethally mutagenized genomes. This could be tested by quantifying viral genomes using quantitative real-time PCR in comparison to infectivity in culture supernatants. Although such studies are beyond the current scope, this would provide important proof of concept in the future.

As the desired effect of ExoN inhibitors would be to increase the genomic mutation rate, this could potentially result in a concomitant increase in viral variation, with the potential to create new gain-of-function variants with clinical implications. For this reason, any ExoN inhibitors used clinically would need to be in combination with mutagenic nucleosides such that the mutation rate would be sufficient to induce error catastrophe and not permit the generation of viable, infectious mutated viruses. In this regard, our data confirm that CB3 and CB3-1 synergize with well-characterized mutagenic nucleoside analogues. Having said this, it would be important to choose the appropriate nucleoside analogues as it has been shown that some structural features

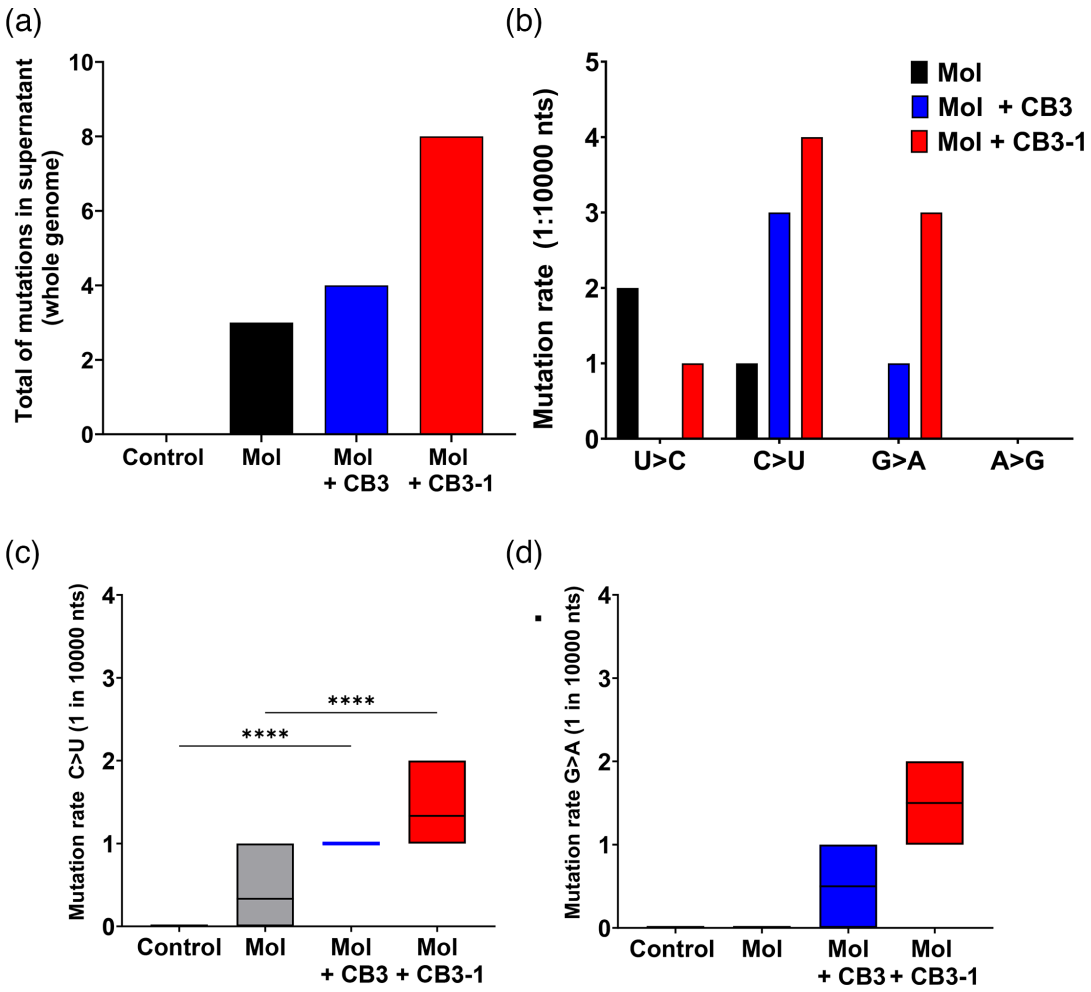

Fig. 8. Determination of CB3/CB3-1 mode of action by WGS analysis. A549-AT cells were infected with SARS-CoV-2 at an MOI of 0.1 in the presence of molnupiravir (EC_{90}) or with the combination of molnupiravir with CB3 or CB3-1. After 24 h, supernatants were then harvested, and total RNA was extracted and submitted to NGS sequencing. The variant calling was performed employing the iVar algorithm allowing the identification of the total number of mutations in the whole-genome sequence (a), and the mutation rate per nucleotide substitution (b). The mutation rate per 10,000 nt for those substitutions that were higher than molnupiravir alone (C>U (c) and G>A (d)) was also compared. Mean values ± SD. ****, $P < 0.0001$ (one-way ANOVA).

of these molecules render them at least partially resistant to the ExoN activity, for example, dideoxynucleotides lacking both 2′ and 3′OH groups [31]. Thus, molnupiravir, which has both 2′ and 3′OH groups, is likely a strong candidate for combination therapy with ExoN inhibitors, exemplified by the data presented here (Fig. 6) showing significant increases in potency of molnupiravir in the presence of either CB3 or CB3-1.

In conclusion, we show that inhibitors of the SARS-CoV-2 ExoN activity have potential as future antiviral agents, in combination with well-characterized (and safe) mutagenic ribonucleotides. Importantly, the high level of homology and conservation of the ExoN structure within coronaviruses means that ExoN inhibitors may also have pan-coronavirus activity and could form part of a future pandemic preparedness strategy.

Funding information
This study was funded by the UK Medical Research Council (grant no. MR/V036904/1) and the COVID-19 Genomics UK Consortium (COG-UK). The Incucyte S3 purchase was funded by a Wellcome Multi-User Equipment grant (221538/Z/20/Z). The funders had no role in study design, data collection and analysis, decision to publish or preparation of the manuscript.

Acknowledgements
We thank Professor Andres Merits (University of Tartu, Estonia) for the SARS-CoV-2 subgenomic replicon plasmid pCCL-4K-SARS-CoV-2-Repl-PL-mNeonGreen.

Author contributions
V.E., M.J.M., C.W.G.F., E.P. and M.H. planned the study. V.E., M.J.M., I.A.S., P.H., C.P.M., S.A. and A.St.J. performed the experiments. V.E., M.J.M., C.P.M. and S.A. analysed the data. V.E., M.J.M. and M.H. wrote the main manuscript text. All authors reviewed the manuscript.

Conflicts of interest
The authors declare that there are no conflicts of interest.

References

1. Woo PCY, de Groot RJ, Haagmans B, Lau SKP, Neuman BW, *et al*. ICTV Virus Taxonomy Profile: Coronaviridae 2023. *J Gen Virol* 2023;104.
2. Denison MR, Graham RL, Donaldson EF, Eckerle LD, Baric RS. Coronaviruses: an RNA proofreading machine regulates replication fidelity and diversity. *RNA Biol* 2011;8:270–279.
3. Bouvet M, Imbert I, Subissi L, Gluais L, Canard B, *et al*. RNA 3'-end mismatch excision by the severe acute respiratory syndrome coronavirus nonstructural protein nsp10/nsp14 exoribonuclease complex. *Proc Natl Acad Sci USA* 2012;109:9372–9377.
4. Tahir M. Coronavirus genomic nsp14-ExoN, structure, role, mechanism, and potential application as a drug target. *J Med Virol* 2021;93:4258–4264.
5. Ogando NS, Zevenhoven-Dobbe JC, van der Meer Y, Bredenbeek PJ, Posthuma CC, *et al*. The enzymatic activity of the nsp14 exoribonuclease is critical for replication of MERS-CoV and SARS-CoV-2. *J Virol* 2020;94:e01246-20.
6. Eckerle LD, Becker MM, Halpin RA, Li K, Venter E, *et al*. Infidelity of SARS-CoV Nsp14-exonuclease mutant virus replication is revealed by complete genome sequencing. *PLoS Pathog* 2010;6:e1000896.
7. Eckerle LD, Lu X, Sperry SM, Choi L, Denison MR. High fidelity of murine hepatitis virus replication is decreased in nsp14 exoribonuclease mutants. *J Virol* 2007;81:12135–12144.
8. Oliveira LS, Rosa LB, Affonso DD, Santos IA, Silva JC, *et al*. Novel bidentate amine ligand and the interplay between Pd(II) and Pt(II) coordination and biological activity. *Chembiochem* 2024;25:e202300696.
9. Gorgulla C, Boeszoermenyi A, Wang Z-F, Fischer PD, Coote PW, *et al*. An open-source drug discovery platform enables ultra-large virtual screens. *Nature* 2020;580:663–668.
10. Hierholzer JCK, Killington RA. Virus isolation and quantitation. *Virology Methods Manual* 2007;2:25–46.
11. McClure CP, Tsoleridis T, Holmes N, Chappell JG, Byaruhanga T, *et al*. Vivaldi': an amplicon-based whole genome sequencing method for the four seasonal human coronaviruses 229E, NL63, OC43 & HKU1, alongside SARS-CoV-2. *Infect Dis* 2024.
12. Dangerfield TL, Johnson KA. Substrate specificity and kinetics of RNA hydrolysis by SARS-CoV-2 NSP10/14 exonuclease. *ACS Bio Med Chem Au* 2022;2:600–606.
13. Li H. Minimap2: pairwise alignment for nucleotide sequences. *Bioinformatics* 2018;34:3094–3100.
14. Grubaugh ND, Gangavarapu K, Quick J, Matteson NL, De Jesus JG, *et al*. An amplicon-based sequencing framework for accurately measuring intrahost virus diversity using PrimalSeq and iVar. *Genome Biol* 2019;20:8.
15. Sali A, Blundell TL. Comparative protein modelling by satisfaction of spatial restraints. *J Mol Biol* 1993;234:779–815.
16. Lin S, Chen H, Chen Z, Yang F, Ye F, *et al*. Crystal structure of SARS-CoV-2 nsp10 bound to nsp14-ExoN domain reveals an exoribonuclease with both structural and functional integrity. *Nucleic Acids Res* 2021;49:5382–5392.
17. Mikhailovskii O, Izmailov SA, Xue Y, Case DA, Skrynnikov NR. X-ray crystallography module in MD simulation program amber 2023. *Refining the Models of Protein Crystals J Chem Inf Model* 2024;64:18–25.
18. Smith EC, Blanc H, Surdel MC, Vignuzzi M, Denison MR. Coronaviruses lacking exoribonuclease activity are susceptible to lethal mutagenesis: evidence for proofreading and potential therapeutics. *PLoS Pathog* 2013;9:e1003565.
19. Moeller NH, Passow KT, Harki DA, Aihara H. SARS-CoV-2 nsp14 exoribonuclease removes the natural antiviral 3'-deoxy-3',4'-didehydro-cytidine nucleotide from RNA. *Viruses* 2022;14:1790.
20. Deval J, Gurard-Levin ZA. Opportunities and challenges in targeting the proofreading activity of SARS-CoV-2 polymerase complex. *Molecules* 2022;27:2918.
21. Rihn SJ, Merits A, Bakshi S, Turnbull ML, Wickenhagen A, *et al*. A plasmid DNA-launched SARS-CoV-2 reverse genetics system and coronavirus toolkit for COVID-19 research. *PLoS Biol* 2021;19:e3001091.
22. Menéndez-Arias L. Decoding molnupiravir-induced mutagenesis in SARS-CoV-2. *J Biol Chem* 2021;297:100867.
23. Francis RV, Billam H, Clarke M, Yates C, Tsoleridis T, *et al*. The impact of real-time whole-genome sequencing in controlling healthcare-associated SARS-CoV-2 outbreaks. *J Infect Dis* 2022;225:10–18.
24. Canal B, McClure AW, Curran JF, Wu M, Ulferts R, *et al*. Identifying SARS-CoV-2 antiviral compounds by screening for small molecule inhibitors of nsp14/nsp10 exoribonuclease. *Biochem J* 2021;478:2445–2464.
25. Baddock HT, Brolih S, Yosaatmadja Y, Ratnaweera M, Bielinski M, *et al*. Characterization of the SARS-CoV-2 ExoN (nsp14ExoN-nsp10) complex: implications for its role in viral genome stability and inhibitor identification. *Nucleic Acids Res* 2022;50:1484–1500.
26. Khater S, Kumar P, Dasgupta N, Das G, Ray S, *et al*. Combining SARS-CoV-2 proofreading exonuclease and RNA-dependent RNA polymerase inhibitors as a strategy to combat COVID-19: a high-throughput *in silico* screening. *Front Microbiol* 2021;12:647693.
27. Asthana A, Corona A, Shin W-J, Kwak M-J, Gaughan C, *et al*. Analogs of the catechol derivative dynasore inhibit HIV-1 ribonuclease H, SARS-CoV-2 nsp14 exoribonuclease, and virus replication. *Viruses* 2023;15:1539.
28. Rona G, Zeke A, Miwatani-Minter B, de Vries M, Kaur R, *et al*. The NSP14/NSP10 RNA repair complex as a Pan-coronavirus therapeutic target. *Cell Death Differ* 2022;29:285–292.
29. Wang X, Sacramento CQ, Jockusch S, Chaves OA, Tao C, *et al*. Combination of antiviral drugs inhibits SARS-CoV-2 polymerase and exonuclease and demonstrates COVID-19 therapeutic potential in viral cell culture. *Commun Biol* 2022;5:154.
30. Takada K, Ueda MT, Shichinohe S, Kida Y, Ono C, *et al*. Genomic diversity of SARS-CoV-2 can be accelerated by mutations in the nsp14 gene. *iScience* 2023;26:106210.
31. Wang X, Tao C, Morozova I, Kalachikov S, Li X, *et al*. Identifying structural features of nucleotide analogues to overcome SARS-CoV-2 exonuclease activity. *Viruses* 2022;14:1413.